

Article

Characterization of Coloured Gemstones by X-ray Micro Computed Tomography

René Heyn ^{1,*}, Abraham Rozendaal ¹, Anton Du Plessis ²  and Carene Mouton ¹

¹ Department of Earth Sciences, Stellenbosch University, Stellenbosch 7602, South Africa; ar@sun.ac.za (A.R.); 18695612@sun.ac.za (C.M.)

² Department of Physics, Stellenbosch University, Stellenbosch 7602, South Africa; anton2@sun.ac.za

* Correspondence: rheyne@sun.ac.za

Abstract: The monetary value of gemstones is based on five variables: rarity, cut, weight, color and clarity. The latter refers to internal impurities and defects. Fashion may also dictate demand and price. To enhance some of these features and value, gemstones are treated. Disclosure or nondisclosure thereof has been controversial and affected consumer confidence. Most of these treatments are difficult to detect with the naked eye and accurately quantify with traditional optical and analytical methods. X-ray micro computed tomography (micro-CT or μ CT) is proposed as a relatively low cost, physically non-destructive and complementary method to detect and quantify clarity enhancement and also to provide a unique 3D fingerprint of each gemstone. A collection of 14 cut colored gemstones was selected. Micro-CT scans allowed fracture detection, their distribution and calculation of filler volume as well as 3D mapping of inclusions, surface and internal imperfections and artificially induced modifications. As a result the method allows the construction of a digital twin. X-ray exposure could however induce unwanted color changes. This effect was minimized or eliminated by optimizing dosage and exposure time.

Keywords: gemstones; X-ray computed tomography; fingerprinting; quality control



Citation: Heyn, R.; Rozendaal, A.; Du Plessis, A.; Mouton, C. Characterization of Coloured Gemstones by X-ray Micro Computed Tomography. *Minerals* **2021**, *11*, 178. <https://doi.org/10.3390/min11020178>

Received: 19 November 2020

Accepted: 19 January 2021

Published: 8 February 2021

Publisher's Note: MDPI stays neutral with regard to jurisdictional claims in published maps and institutional affiliations.



Copyright: © 2021 by the authors. Licensee MDPI, Basel, Switzerland. This article is an open access article distributed under the terms and conditions of the Creative Commons Attribution (CC BY) license (<https://creativecommons.org/licenses/by/4.0/>).

1. Introduction

1.1. Background

Due to the limited availability and significant cost of high quality natural gemstones, the market for more affordable gemstones has expanded. In recent years, major advances in gemstone synthesis and treatment by which the appearance and durability can be enhanced, has become increasingly customary for most major gemstone materials [1–3]. The clarity of a gemstone decreases with the presence of small cracks or fractures and mineral inclusions. The presence of inclusions in a colored gemstone and lately diamonds are essential in order to certify the stone as natural [4]. With heat treatment, inclusions may decrease in size or diffuse into the host material, thereby improving its clarity. Low-clarity fractured gemstones are usually enhanced by fracture filling. A variety of fracture filling materials with refractive indices near that of the gemstone host, can aid to avoid reflection of the fracture surface and thereby reduces unwanted light scattering [5]. A close match makes fractures virtually invisible and may significantly increase the value of inherently poor quality gems. Corundum (Al_2O_3) for example, a hard and very durable mineral, lends itself to many treatments. Ruby, the red most valued color of corundum, is often a prime focus of these treatments. Fractures are commonly filled with a lead-based glass of a high refractive index similar to that of corundum and can alter highly fractured, almost opaque, red corundum with no gem value into translucent and even transparent gem rubies. In general, the filler may vary from solids to liquids and are not always stable or durable. This results in damage to gems and loss of value during jewelry manufacturing or normal use during its lifetime [6–8].

1.2. The Market and Characterization

The lack of disclosure or the concealment of gemstone treatment has negatively influenced the gemstone market by decreasing consumer confidence [9]. Greater transparency and knowledge of gemstone treatment has however, restored public confidence. Most auction houses have adopted full disclosure policies, informing customers whether gems have been artificially enhanced based on trade disclosure regulations by CIBJO, the World Jewelry Confederation [10,11]. This created a need to apply observational and interpretational skills to detect gemstone enhancements with more sophisticated analytical instruments than an optical microscope or hand held loupe. These include infrared and ultraviolet-visible spectrometers, energy-dispersive X-ray fluorescence, X-ray diffraction and Raman microscopy instrumentation. In addition, the use of techniques providing chemical analysis with low detection limits, such as secondary ion mass spectrometry, laser ablation-inductively coupled plasma-mass spectrometry and laser induced breakdown spectroscopy became essential [3,12]. It remains essential however, that alternative, but complementary methods to all the above are developed that are preferably non-destructive and provide accurate results at reasonable cost.

A debate has emerged in the gemstone industry around the amount of artificial material deemed appropriate in a fracture-filled gemstone. Scarratt [13] discussed the discrepancy between the definition of a treated and a manufactured gemstone. If an artificial material (such as glass) becomes the dominant constituent used during a treatment process, then the end-product may not be considered a treated gemstone, but instead as a manufactured product. The challenge for the gemmologist is to quantitatively determine the weight of the dominant constituent to make the distinction. The result could have value implications.

In the case of diamonds, a grading report accompanies almost every stone being sold by a reputable seller, with information on its cut, clarity, color and carat weight [14]. The four C's as it is known provides the consumer with the characteristics of a specific stone. The colored gemstone market has not reached that level of sophistication probably only from the high end of the market. Designers and dealers provide the caratage only, without a laboratory report containing other diagnostic features of the stone. Even if a colored stone identification report is provided, the contents can differ from laboratory to laboratory [15]. The results of this study can contribute to more detailed and reliable gemology reports.

1.3. X-ray Micro Computed Tomography (μ CT)

Micro-CT is a non-destructive three-dimensional visualization and characterization method that allows the user to study the external and internal structure of an object with high spatial resolution. It is a fast advancing technology of proven significance in gemological research as evidenced by studies of natural pearls [16–19] and rubies [20–22]. Materials or phases with different x-ray densities are depicted in different shades of grey. As a result, the distribution of inclusions, fractures, internal defects, and impurities, as well as surface features of gems can be easily distinguished (Figure 1). Despite the high cost of μ CT hardware, it is a technology used in a wide variety of applications such as geosciences [23–25], materials science [26], civil engineering materials [27], biological applications [28], herpetology [29], biomimicry [30] and additive manufacturing [31]. This broad application ability has resulted in increased availability in the form of service laboratories all over the world. Small desktop models are also available which could be used by individual gem laboratories.

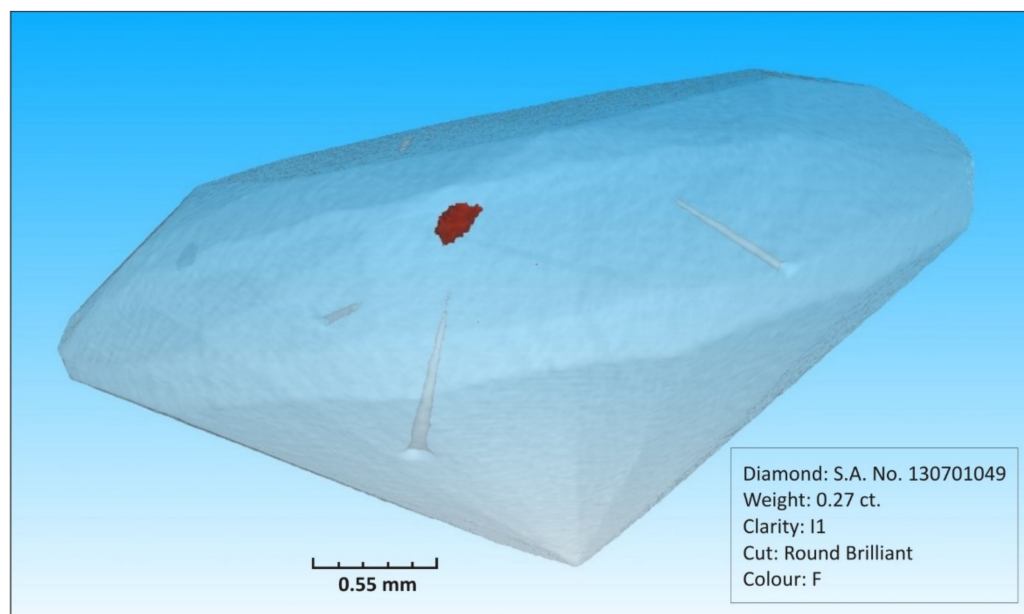


Figure 1. A 3D computed tomography (CT)-scan image of a diamond revealing drill channels and an inclusion, modified after Roux [32].

By using μ CT, this study attempts to develop a safe and accurate method to characterize individual colored gemstones by the detection and identification of interior and exterior imperfections as well as the volume calculation of artificial fissure filling material when present in a gemstone. This will allow the presentation of a unique “fingerprint” of each gemstone. A preliminary study on the μ CT analysis of cut and polished diamonds [33,34] revealed that temporary discoloration occurred after exposure to relatively high dosages of X-ray radiation. The present study further reports on the safe dosages of X-ray radiation on various colored gemstones during μ CT analyses.

2. Materials and Methods

The present study used fourteen colored gemstones, which have been obtained from the gemstone collection at the University of Stellenbosch, the European Gemological Laboratory (EGL) in South Africa or purchased in the open market (Table 1). In addition to weight in carat the girdle diameter was also specified as an indication of size because of density variations of the gemstones. Gemstones were selected with the specific purpose to experimentally test the effectiveness or otherwise of the μ CT method. To this end stones of relatively low monetary value, with extreme fracture distribution and high density filling such as lead glass to ensure high fill-host contrast, were selected for this purpose. Ruby was selected to quantify fracture-filling volume as this is a common treatment method of these gemstones. These include the glass-filled ruby, which is fracture-filled with a highly refractive leaded glass and the EGL ruby which is fracture-filled with a high density (lead) glass substance. A blue diffused sapphire (Sample A, Table 1) together with the abovementioned rubies, was selected to determine their “unique fingerprints”. Twelve gemstones were used to test the effect of X-ray exposure on their color (Table 1).

Instrumentation used include a General Electric Phoenix VTomex L240/NF180 and a Nanotom S (General Electric, Wunstorf, Germany). The latter has a lower power X-ray tube that is very stable over long periods and ensures sharper images of small samples (such as gems) [35]. Operating conditions varied depending on the resolution of the images required. To minimize image artifacts such as sample movement during scanning causing blurred images [36], each gemstone was mounted on a small cube of polystyrene. This was fixed onto a glass rod to hold the gemstone in place on the rotation stage. Samples

were positioned at a slight angle in the CT scanner to prevent image artifacts and improve detail [28].

Table 1. Gemstones used in this study.

Sample Name (Commercial Name)	Mineral	Diameter	Approximate Carat Weight	Cut	Treatment	Experiment
Pb-glass-filled Ruby	Corundum	5 mm	0.63	Round brilliant	Fracture filled	1,2,3
EGL Ruby	Corundum	11 × 7 mm	2.65	Pear brilliant	Fracture filled	1,2
Diffusion treated sapphire A	Corundum	3 mm	0.13	Round brilliant	Heat treated	2,3
Diffusion treated sapphire B	Corundum	3 mm	0.13	Round brilliant	Diffusion treatment	3
Diffusion treated sapphire C	Corundum	3 mm	0.13	Round brilliant	Diffusion treatment	3
Yellow sapphire	Corundum	8 × 6 mm	1.36	Round brilliant		3
Indian Ruby A	Corundum	7 mm	1.58	Round brilliant		3
Indian Ruby B	Corundum	7 mm	1.58	Round brilliant		3
Indian Ruby C	Corundum	7 mm	1.58	Round brilliant		3
Emerald (Colombian)	Beryl	7 mm	1.67	Round brilliant		3
Topaz A (London blue)	Topaz	6 mm	0.83	Trillion		3
Topaz B (Sky blue)	Topaz	6 mm	0.83	Trillion		3
Hydro Amethyst	Quartz	12 mm	5.67	Cushion rose cut		3
Tanzanite	Zoisite	8 × 5 mm	2.14	Cabochon		3

Experiment 1 = Quantify the fracture filling volume; Experiment 2 = Determine a “unique fingerprint”; Experiment 3 = Test the effect of X-ray exposure on the color of the gemstones.

Images of the EGL ruby were acquired with the nano-CT scanner operating at 130 kV and 40 μ A with a copper beam filtration of 0.1 mm. Voxel size was 5 μ m and the image acquisition time set to 500 milliseconds per image. The images were recorded in 4800 rotation steps during a rotation of 360°. To improve image quality, the first image was discarded at each step and the following three images were averaged. This was standard procedure for both micro and nano scans.

The glass-filled ruby as well as the blue diffused sapphire A (Table 1) were analysed also using the nano-CT scanner but applying a voltage of 100 kV, a current of 50 μ A and a copper beam filtration of 0.1 mm. The voxel size was set to 7.5 μ m with an image acquisition time of 500 milliseconds per image and were recorded in 2400 rotation steps during a 360° rotation of the sample.

Ring artifacts typically result due to rotation of the samples during scanning and are visually encountered as rings around the center of rotation on slice images [28]. The detector shift was activated in all three scans to minimize these ring artefacts, whereas the automatic scan optimizer was enabled to eliminate artifacts or blurred images caused by potential sample movement or X-ray spot drift.

The images generated were used to define 3D images, which allowed mapping of the natural as well as artificially induced internal imperfections and generating a fingerprint of each gemstone.

2.1. Fracture Filling

To quantify lead glass fracture-filling, the methodology used by le Roux et al. [37] to determine tungsten ore grade with micro-CT was used. Image analyses used Volume Graphics VGStudioMax 3.0 and reconstructions were completed in system-supplied Datos reconstruction software. For the 3D data analysis, the entire gemstone is selected with a

region growing tool to remove the surrounding air. The resultant histogram in greyscale, contains only two dominant peaks. In interval 1 with low values, the peak represents the bulk host ruby and the peak in interval 2 the denser filling material (Figure 2). The filling material and bulk host ruby is separated by a vertical segmentation line (threshold) positioned at the bottom dip of the histogram, in the middle of the two dominant peaks (a variation of the widely used iso-50 global threshold). A further advanced surface fit is performed on the region of interest (ROI), to ensure the inclusion of all greyscale values from the denser filling material, which uses the global segmentation line as a starting point. A local threshold gradient search is performed in the region of the global threshold, to detect the sharpest change in grey value at the region boundary [37]. The produced fracture filling ROI can be used to make volumetric measurements [37]. Once the percentage of filling material has been calculated, the gemstone can be characterized as either treated or manufactured.

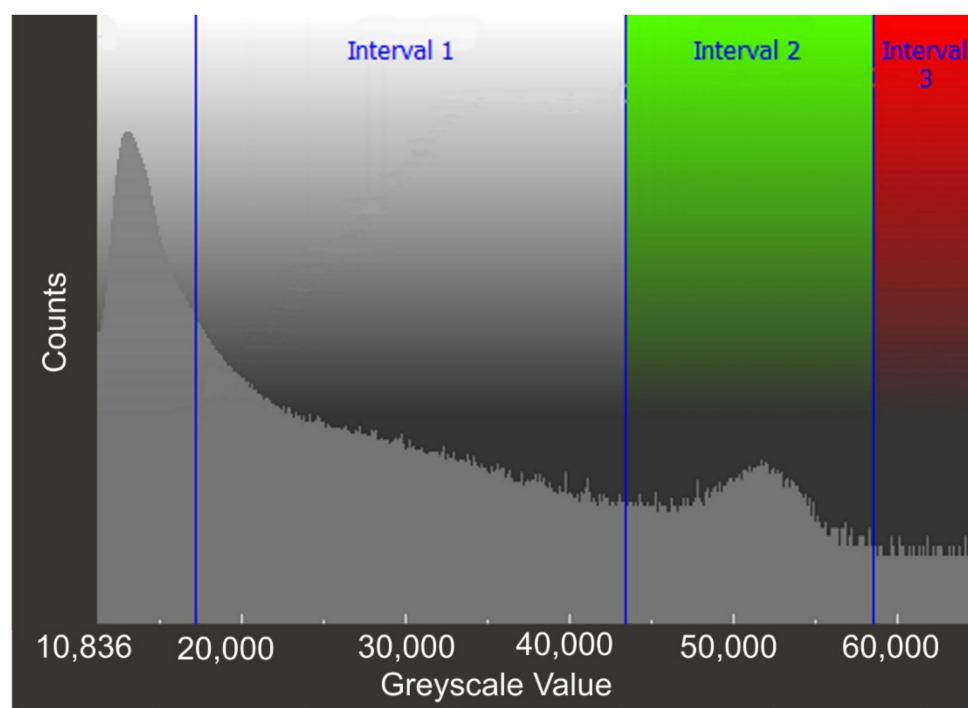


Figure 2. Diagram showing the initial segmentation used to select the greyscale values associated with the fracture filling material of the glass-filled ruby. It is a density separation. Interval 1 (grey) peak is the bulk host gem material and Interval 2 (green) peak is the filler. Interval 3 is filler-related denser material.

2.2. Fingerprint

The same segmentation method as described above was used to produce a unique fingerprint of each gemstone. A surface determination function was applied, and the selected surfaces were converted into 3D triangular polygon mesh (STL) files with the 'normal with simplification' parameter. Two separate mesh files were created for the glass-filled ruby, based on slightly different threshold values. This was to determine whether different threshold values, producing slightly different mesh sizes, would influence the overlap. The 'best fit registration' tool was used to compare the mesh files.

2.3. Colour Change

Exposure to X-rays may induce a color change in gemstones, which may enhance or reduce its monetary value. X-ray irradiation affects the crystal structure defects of minerals, which act as color centers. These defects become trap sites for the electrons freed from

halogen ions after the X-ray exposure. Additional absorption of optical light photons of certain energies then result due to the recharge of these structural defects and the change of valence orbitals [38,39]. In micro-CT studies color change of gemstones should be prevented. To investigate this effect in practice with gemstones, thirteen of the gemstones have been selected from the suite (Table 1). Discoloration was deliberately induced with high dosages. The glass-filled ruby and the Sky Blue topaz A were exposed to high dosage X-rays and 'harsh' scanner settings, atypical of regular CT-scans. The glass-filled ruby was scanned with the Direct Tube (General Electric, Wunstorf, Germany), which is a high power microfocus X-ray source (reflection-type source design) in the micro-CT system. It operates at 200 kV, with a current of 200 μ A with no filter and a distance of 20 mm between the sample and the X-ray source (ZS-distance) was set. This was done over a period of 10 min. The Sky Blue topaz A was also scanned for 35 min at 200 kV, with a current of 800 μ A with no filter and a ZS-distance of 16.3 mm. The induced color changes may regress when exposed to sufficient UV-rays or heat treatment (such as hot water). This is because the induced charges in the irradiated gemstones are usually unstable in the crystal lattice [38,39]. In the present study, the glass-filled ruby and Sky Blue topaz A were submerged in boiling water for 5 min shortly after scanning. This was to determine if the discolorations were almost immediately reversible. The encountered discoloration was also monitored over a seven-month period to determine whether the changes are temporary or permanent.

To establish whether gemstone color will be affected by X-ray exposure during a routine CT-scan, various samples from the collection were scanned under 'typical' CT conditions, following the guidelines of du Plessis et al. [28]. These included three blue diffused sapphires, three natural Indian rubies, Colombian emerald, London Blue topaz, laboratory-grown hydro amethyst, yellow sapphire and tanzanite (Table 1). Gemstones were scanned at 100 kV, with a current of 200 μ A. The smaller the distance between the sample and the source (ZS-distance), the more x-ray irradiation exposure of the sample is achieved. To minimize exposure the ZS-distance was increased to 600 mm and scanned at 10 μ m resolution, while the sample rotates through 360° to imitate a standard scan. A 0.1 mm copper filter was used on the X-ray beam. A scan time of five minutes was considered sufficient to generate measurable data and acceptable images with minimal X-ray exposure [35].

The visible-light reflection spectra of each gemstone was recorded using a calibrated Ocean Optics USB4000 Spectrometer (Ocean Insight, Rochester, New York, USA) before and after exposure to X-rays. All gemstones were mounted on a small block of white polystyrene to prevent interference with the generated spectrum and to ensure that the spectrum is recorded from the approximate same reflection plane, i.e., the table of the gemstone.

The samples were irradiated with visible light from an Ocean Optics tungsten halogen light source and optical reflection spectra were recorded with OceanView 1.5.2. spectroscopy software with an integration time of 100 milliseconds. A bifurcated fiber was used for easy delivery of light to the gemstone in a ~m spot and collected with the same fiber for spectral acquisition of transmitted and reflected light. Due to the simplified setup of the instrumentation, it was only possible to provide reflectance spectra. The method did not allow high quality precise measurements to permit quantification of possible slight color modifications induced in gemstones by X-ray exposure, except in extreme cases such as the Sky Blue topaz. Clearly more research with more advanced instrumentation is required to improve the quality of the data.

3. Results

3.1. Fracture Fill Detection and Volume Calculation

The CT-scan cross-section images and 3D models of the two fracture filled rubies allowed definition of their geometry, surface features and internal fractures. The fracture filling material is clearly visible by its higher density compared to that of the gemstone host.

This is indicated by the voxel grey scale where high density material is lighter and less dense material, the gemstone material, is darker (Figure 3a,b). When fractures have not been filled, the density contrast is reversed. Fracture dimensions in the two rubies varied between broad and narrow interconnected cracks, cross-cutting the entire stone. There are some isolated surface imperfections (Figure 3a,b). The EGL ruby reveals a regular fracture grid pattern that reflects the trigonal crystallographic identity and cleavage/parting directions of corundum. There are two dominant fracture directions intersecting at approximately 80° and are equated with the parting planes $\{0001\}$ and $\{10\bar{1}1\}$. The crown of the ruby was cut at right angles to these two partings and consequently the c-crystallographic axis to optimize polish and reflectivity (Figure 3a). Irregular cross-cutting fractures could be tectonically induced by retrogression and exhumation as well as poorly controlled blasting during mining. This also enhanced the development of parting planes. Although the EGL ruby is homogenous to the naked eye, it has been extensively, albeit successfully treated to conceal its pervasive fracture pattern. The fracture pattern of the glass-filled brilliant cut ruby sample consists mainly of a few randomly orientated, but significant cracks unrelated to the natural cleavage and of tectonic origin. It is clearly less fractured than the EGL ruby (Figure 3b).

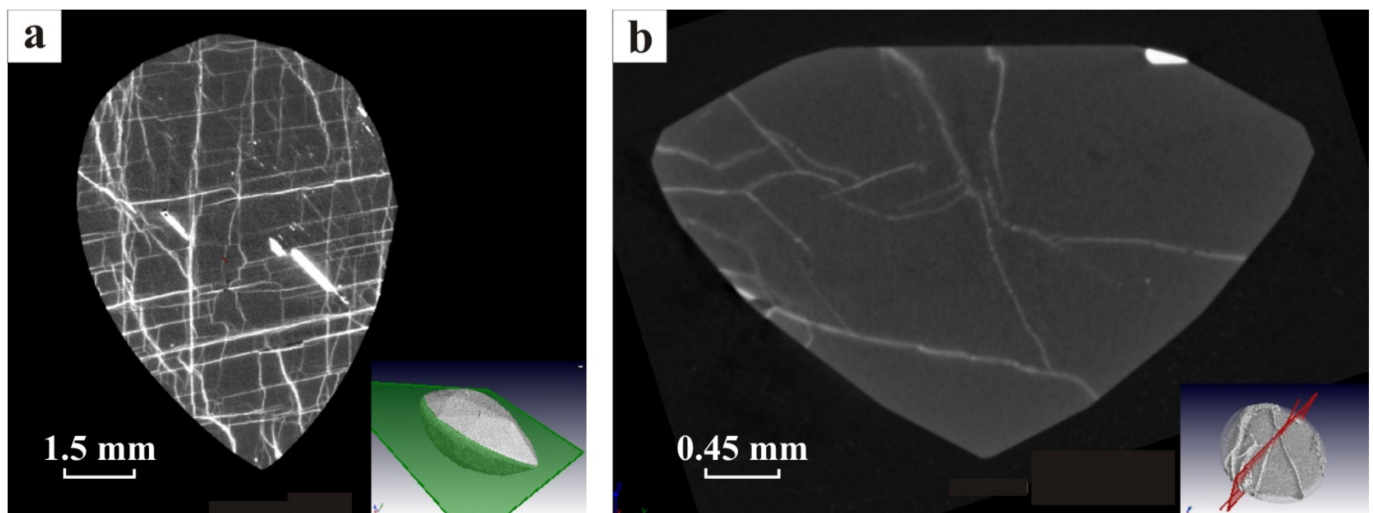


Figure 3. CT-scan section images of the fracture filled rubies, illustrating the less dense host ruby material in grey and the more dense filling material in white to light grey. Position of section planes are shown on the 3D image. (a) The $5\ \mu\text{m}$ resolution scan of the EGL ruby, displays a regular grid pattern of fractures related to the natural cleavage/parting planes of the mineral. (b) The $7.5\ \mu\text{m}$ resolution scan of the m glass-filled ruby displays a random orientation of the fractures.

To quantify fracture dimensions and allow volume calculations, the accurate selection of the greyscale threshold value is imperative. This is done on a greyscale histogram, which contrasts dense and less dense material (Figure 4). Segmentation of fractures is challenging due to the partial volume effect and therefore variations of grey scale values near narrow fracture regions, this is demonstrated in Figure 4a–d. A line distance profile of filled cavity 1 shows a well-defined outline of a dense material on the greyscale histogram (Figure 4a,b). When the selected local threshold is applied to the CT-scan image the high-density area generated, indicated in green, does not fully enclose the filled cavity outline, displaying a white rim (Figure 4b). This suggests that the selection of threshold was most probably a few greyscale values too high and the material classified as bulk host ruby includes voxels of the denser filling substance and results in a small gradient edge (0.8 to 1.1 mm, Figure 4a). As a result, it will under-estimate the volume of the filled cavity. A second filled cavity shows a more complex greyscale histogram (Figure 4c,d). The first conservative iteration (red area) completely under-estimated the threshold positions. When the lower greyscale values are included (green area), it showed an improved fit with the CT image. Similarly,

the white rims surrounding the green filling areas (Figure 4b), revealed as peaks adjacent to the classified greyscales (0.3 to 0.4 mm, Figure 4a) should also be included as filling material, but, once again, the threshold value was set a few greyscale values too high. More iterations are required to optimize the threshold values, secure a best fit and minimize subjectivity with respect to volume calculations.

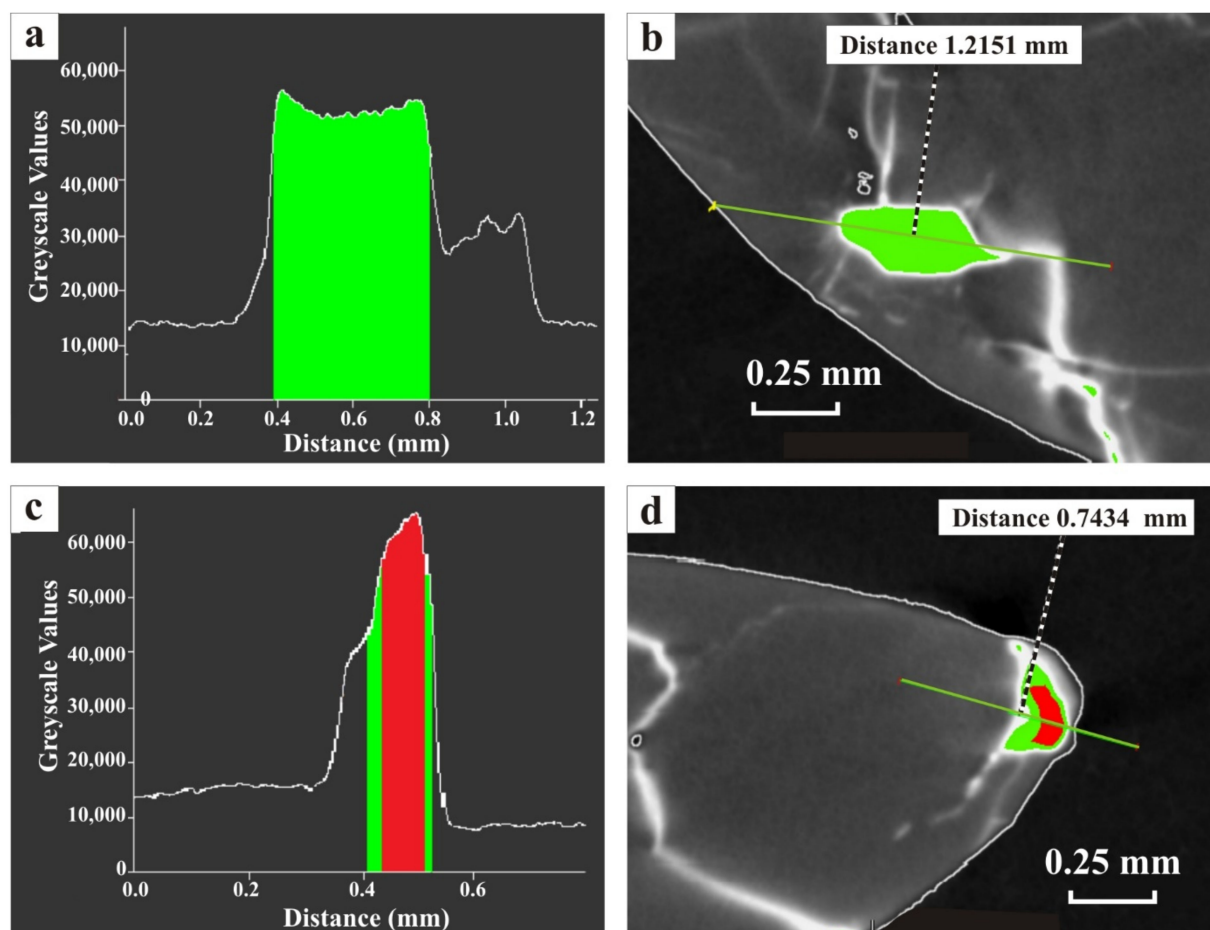


Figure 4. Line distance profile of filled cavity 1 (a) and filled cavity 2 (c) with their respective CT scan images of the cavities (b,d) in the m glass-filled ruby. Different densities are indicated on the greyscale histograms. Cavity 1 displays only one denser filling material (green) while cavity 2 displays two different greyscale density filling materials (red and green) due to the under-estimation of the threshold position.

The volume of the filler within the highly fractured EGL ruby was automatically calculated on the ROIs produced from the global segmentation method following the basic principles discussed above. To compare resolution sensitivity both the 5 μm and 10 μm scans were used (Table 2).

Table 2. Fracture filling volume calculations obtained from the μm CT scans of the European Gemological Laboratory (EGL) ruby.

CT-Scan Resolution	Volume of Entire Stone (mm^3)	Volume of Fracture Filling Material (mm^3)	Percentage Fracture Filling Material
10 μm Scan	148.03137	19.18086	12.957%
5 μm Scan	148.24036	10.15460	6.85%

Figure 5 displays the 3D CT-scan images of the EGL ruby (5 μm scan) and the extracted ROI produced by the segmentation method. The distribution and dimensions of the

fractures are enhanced with a color-coded fracture filling diameter analysis. The most extensive fractures with the largest diameter are indicated in red and the smaller, isolated fractures representing the cavities, are indicated in blue (Figure 5b). Table 2 contains the volume estimates obtained from the two different resolution scans. The significant variation between the fracture filling volumes of the two different scans indicate that resolution does indeed influence the results. This is expected for small features such as fractures. A volumetric proportion of 13% was obtained from the 10 μm scan, compared to the 7% produced from the 5 μm scan. This difference can be ascribed to overestimation of the fracture size with the 10 μm scan due to increased voxel size. The subjectivity of the analyst in selecting thresholds could also play a role. Segmentation and interpolation of greyscale values between voxels will introduce some error when delineating fractures and cavities above a particular threshold value. Cracks that are smaller than the voxel spacing will not be observed, whereas the segmentation line will overestimate more extensive fractures because of finite voxel size and the resultant overlap (Figure 6). Consequently, this method can only be applied to cracks wider than the resolution size. The accuracy of the volume quantification thus increases with the resolution of the scan. To classify gemstones as: gemstone with filling, composite or clarity enhanced, the calculated filler volume range of 7–13% for the EGL ruby is probably acceptable. As a result, the EGL ruby can be classified as a corundum with glass-filled fissures and cavities (category F1; C1) and not a manufactured product according to the Laboratory Manual Harmonization Committee, responsible for the harmonization of gemological report language [40].

Although a CT-scan is able to provide a detailed 3D-image of both surface and internal features of a gemstone it cannot analyze the chemistry of inclusions or fillers. Density calibration however, allows for specific density determinations, which can be used for identification purposes and hardness determination [41]. The CT-scans can be used to identify surface-reaching fractures and energy dispersive X-ray fluorescence (EDXRF) or scanning electron microscope (SEM) analyses can then subsequently identify the various filler types.

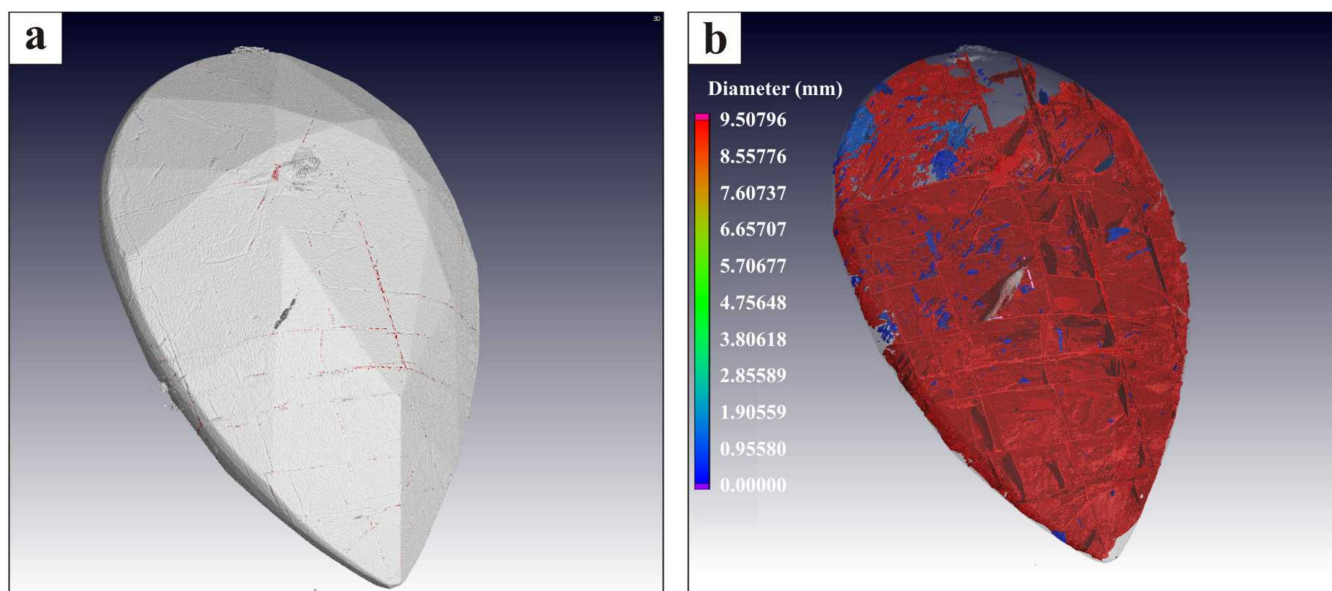


Figure 5. 3D CT-scan images of the EGL ruby (5 μm scan), showing the surface (a) and the results of a color coded fracture filling diameter analysis (b). The largest, interconnected fractures are indicated in red, whereas the smaller, isolated fractures and cavities are shown in blue.

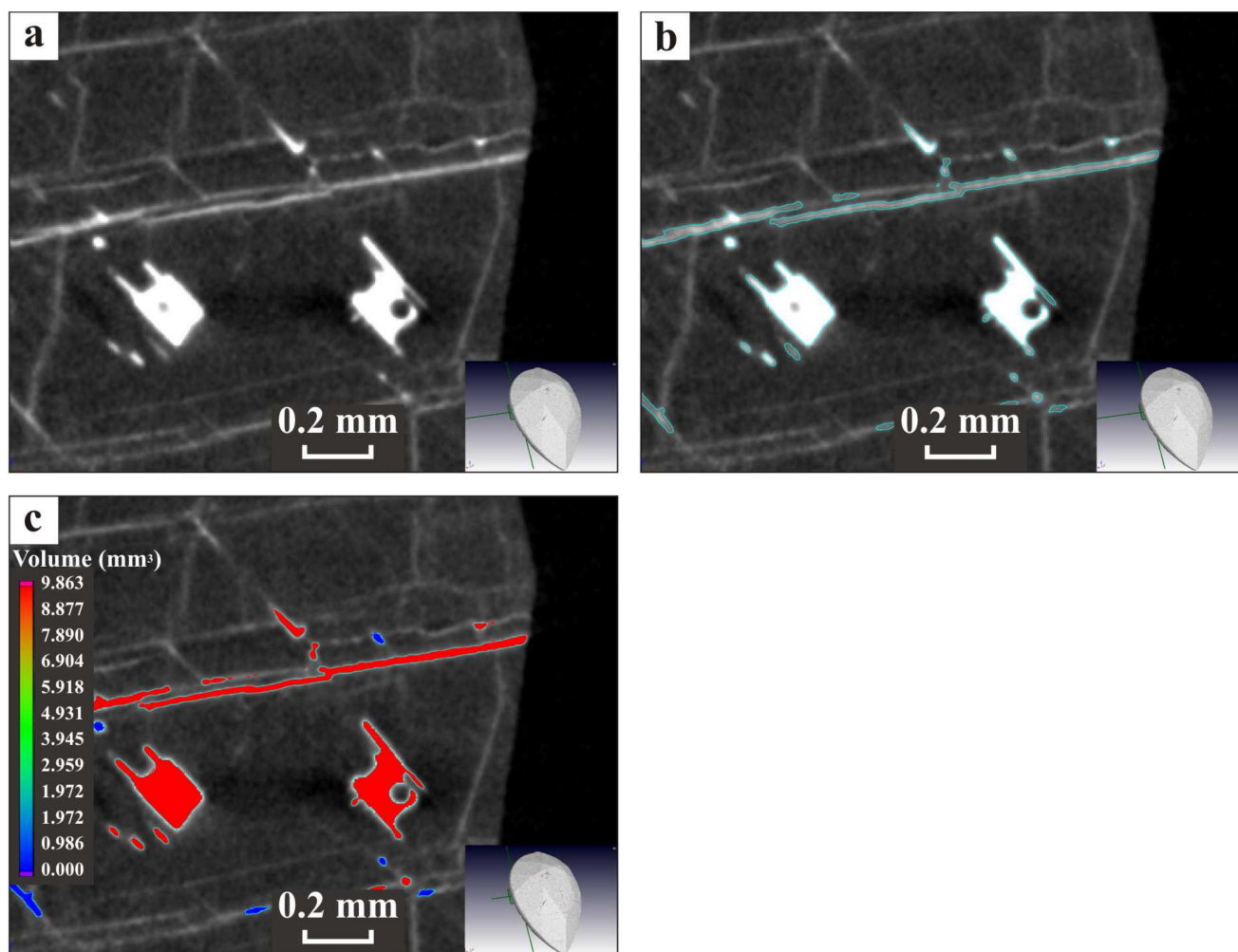


Figure 6. Images of the fracture filled EGL ruby (5 μm scan) depicting the segmentation method used for various sized fractures (light grey/white). Position of section image is shown on 3D image insert. (a). Various sized fractures are segmented and blue lines show areas selected as ROIs (b). The smaller fractures are not segmented, but for the larger fractures the volume is overestimated by including more pixels. The selected areas are extracted as ROIs and color coded according to their volume (c). The blue represents smaller filled areas with red more extensive, interconnected filled fractures.

The X-ray μCT approach is considered complementary to the more conventional methods to determine the geometry and quantity of fractures and quantity of fissure filler such as the gemological microscope and dark field illumination. These traditional methods require examination by a gemological expert and may be unproductive as certain filling materials are difficult to locate and the appearance of some fillers are modified over time [42]. CT analysis does require expert 3D image analysis experience, but analysis procedures can be standardized [8]. Scan times as short as five minutes, despite being noisy, can produce adequate resolution scans and be successfully analysed [43]. Guelpa et al. [41] reported that it is possible to reduce acquisition time and cost further by scanning multiple objects at the same time at a reduced resolution. The resultant scans may still allow for reliable volume and porosity analysis, when these requirements are not critical.

3.2. Producing a Gemstone Fingerprint

Although other methods are available to produce surface and volume meshes [44,45] the present method allowed creating 3D triangular polygon mesh (STL) files of the surface exteriors of gemstones. As a result, a unique fingerprint of each gem was produced. The best-fit registration method was used to study the overlap of the surface meshes of firstly

two totally different stones to validate the method and secondly between two meshes of the same stone to confirm precision. The best-fit registration method automatically inspects meshes for similarities and then aligns these areas for the meshes to overlay. As demonstrated by the lack of overlap between the differing surface meshes of the diffused sapphire A and the EGL ruby the method proved to be robust (Figure 7). The same stone, in this case, the glass-filled ruby was scanned twice to test the method. The method has been demonstrated to be threshold sensitive and analyst subjectivity may incur a deviation between the two 3D images produced (Figure 8). The results show that only minor deviations in the overlap of the two wireframes (Figure 8b) were observed and indicate a slight difference in size. The characteristic features however, remained visible after registration. Thus, mesh files created by different analysts of the same stone, will show the same unique features. When mesh files are generated to illustrate the internal features (defects, inclusions) of a gemstone, the same results are expected. The best-fit registration method will automatically overlay these defining features and confirm their similarity.

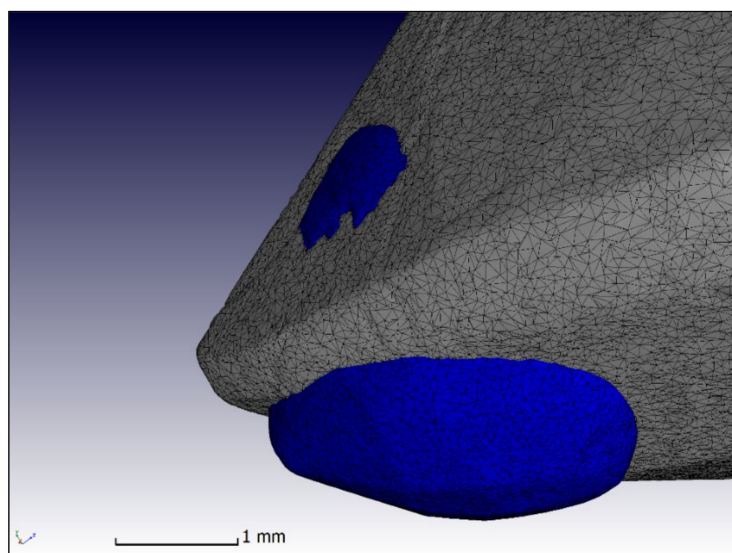


Figure 7. The best-fit registration of the diffused sapphire A exterior surface mesh (blue) with that of the EGL ruby exterior surface mesh (grey) illustrates the dissimilarities between the two stones.

The methodology discussed above is an original procedure and can be developed into a powerful tool to define the unique fingerprint of a gemstone in 3D. It can be done with precision and will be able to confirm the authenticity of a particular stone. The 3D image and fingerprint, the so-called “digital twin” can be a valuable addition to the report that defines the characteristics such as type, origin, treatments, cut, shape, weight and color of a gemstone [46]. A 3D mesh file can also be used to generate a 3D-printed replica of the gemstone.

The CT-scan generated fingerprint can form part of a database for future reference as a digital record or “digital twin”. The GIA database, with information on more than 100,000 individual colored gemstones, is an example of such a reference system which contains the identification records of gems from around the globe [46]. The CT-scan fingerprint complements existing methods and could be an important addition to the GIA database or alternatively, a global standardized fingerprinting record of colored gemstones could be created. Such a digital database can be used to confirm authenticity of stolen/lost gemstones for forensic and insurance purposes by the use of a CT-scan.

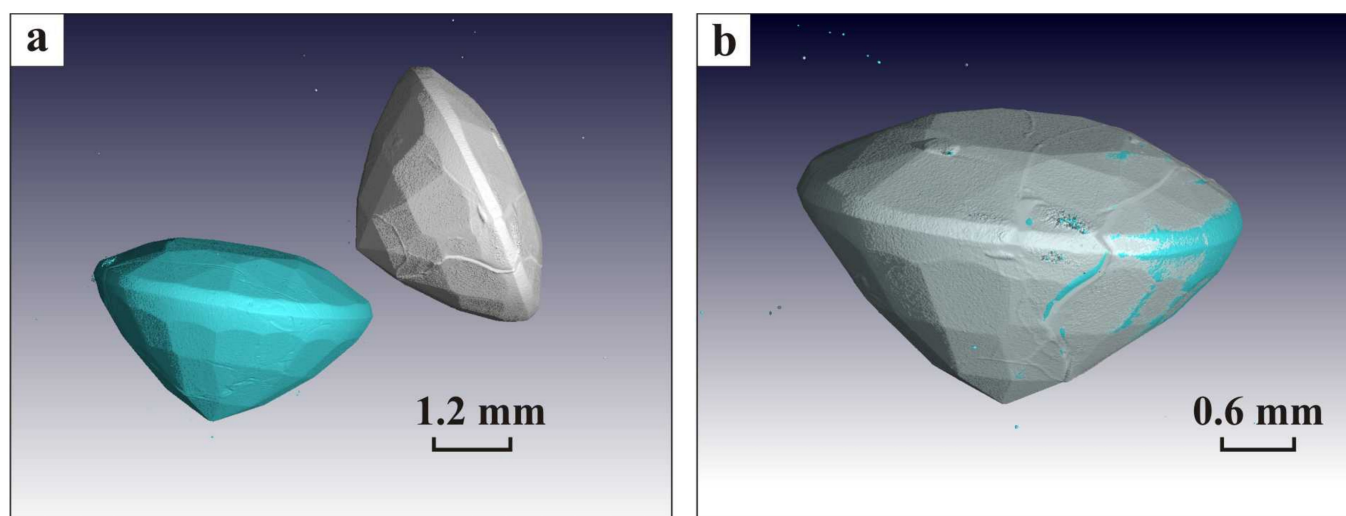


Figure 8. Images of the 3D mesh files created on the exterior surface of the glass-filled ruby. (a) Two iterations at slightly different threshold values produced mesh files indicated in blue and grey. (b) The overlap of the two mesh files after using the best-fit registration method. Slight deviations between the two wireframes are shown where the blue mesh protrudes the grey mesh. Distinct features and their overlap remain visible.

The drawback of this method however, is that the mesh files can be large and their production is time consuming and hence expensive. In the case of the EGL ruby the STL file generated 5 μ m scan is 5.5 gigabytes compared to 34 megabytes of the 10 μ m scan. These are examples illustrating challenges, all of which can be overcome with appropriate guidelines. For example, lower resolution scans are recommended and de-noising image filters are suggested to create a reasonably-sized mesh file. If a stone is recut or polished, the newly generated surface exterior mesh would not fit the older version because of these modifications. The internal features such as inclusions and fractures will however remain preserved and confirm the pre-polish fingerprint. Heat-treatment to recrystallize the internal structure such as cavities or ablated to dissolve inclusions will potentially destroy the internal fingerprint, but surface features may be discernible [2].

3.3. Colour Change Detection

The primary aim of the study is to introduce X-ray μ CT to the gemstone industry as a non-destructive method to characterize gemstones. Consequently, it is essential to prevent potential damage or color changes, due to formation of color centers, to stones caused by the exposure to X-rays [39,47]. To examine this effect, a series of gemstones were exposed to different X-ray dosages and scan times (Table 1). The results show that reflection spectra, before and after the scans under standard conditions with scan times of five minutes, produces insignificant alteration of the primary color. High X-ray dosages and long scanning times however, resulted in semi-permanent discoloration. The experiment deliberately exposed the m glass-filled ruby and the Sky Blue topaz (B) to severe X-ray dosages. The color of the ruby changed from the original pinkish red to a brighter shade of red (Figure 9a,b). This color change persisted after treatment in boiling water. After seven months remnants of the bright red color were still visible. The Sky Blue topaz (B) lost its color and became smoky grey. As with the ruby, boiling water had no effect and only after seven months did some of the blue shades return (Figure 9c–e). The changes observed in the visible light reflection spectra for the Sky Blue topaz indicated that reflection peaks in the blue range (455–492 nm) were eliminated by the high X-ray dosage (Figure 10) [37]. Consequently, X-ray exposure induced the absorption of photons with energies corresponding to the wavelengths of blue light, which is approximately 2.5–2.7 eV [38,48].

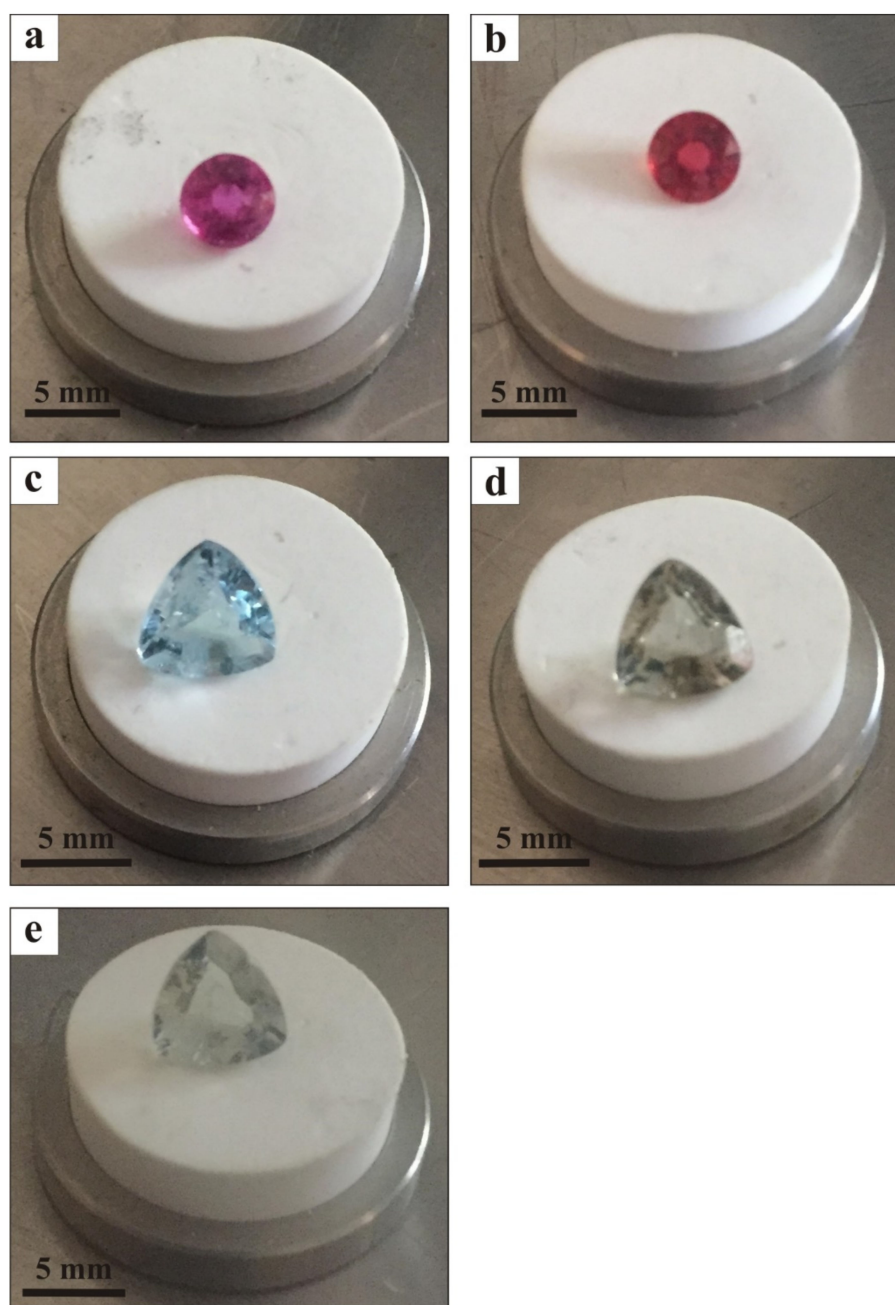


Figure 9. The m glass-filled ruby shows color change after exposure to extreme X-ray dosage (a,b). The Skye Blue topaz (a) lost most of its color during extreme radiation (c,d) and despite hot water treatment and a seven-month recovery period the color was not fully restored (e).

Minimal to no color changes were observed after subjecting various colored gemstones to five-minute scans with typical CT-scanner settings. It was previously demonstrated that such scans can produce dependable results for the purpose of gemstone classification with minimal exposure to X-rays [34]. The resolution of the visible light reflection spectra was not high enough to reliably quantify the before and after radiation exposure differences.

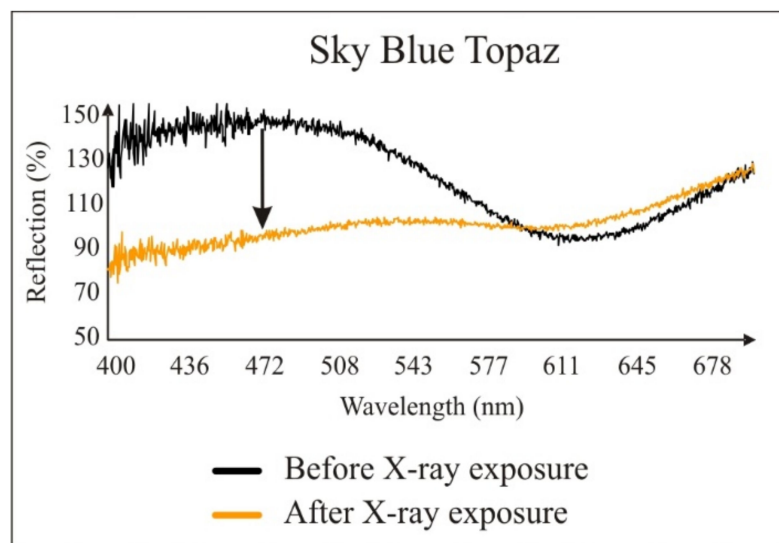


Figure 10. Visible light reflection spectra of the Sky Blue topaz before and after X-ray exposure. Reflection peaks in the blue range (455–492 nm) were eliminated.

4. Discussion

This study demonstrates that X-ray micro computed tomography can make a positive contribution to the characterization and classification of colored gemstones. It has the ability to image by means of 3D polygon mesh files, both external and internal features. These include surface imperfections, poor cut and poor polish. Internally the shape and size of natural and induced fractures and partings, laser holes to ablate inclusions as well as inclusions and cavities, can be detected. In addition, a CT-scan and supporting software allows the detection of fracture filling material and their volumetric determination, provided the density difference between the host stone and the filling material is adequate such as for example lead glass filler. This allows the classification of a gemstone either as treated or manufactured. The combination of external and internal 3D image characteristics defines the unique properties or fingerprint ID of each individual gemstone. This has been defined as the “digital twin”. These attributes of X-ray CT can find its application in the classification of a gemstone and the 3D files as an addendum, which is complementary to the methods (e.g., microscopy) used in the more traditional gemstone report. It is able to identify subsequent modifications to a classified stone or accidental/wilful replacement by means of the best fit registration method.

X-ray micro computed tomography applied to gemstones is however, in its development stage. Permanent to semi-permanent color changes are induced by exposure to severe x-ray bombardment. The preliminary results of this study demonstrate that by limiting the exposure time to five minutes under standard operating conditions, insignificant or no color damage has been detected. This renders the method as safe for gemstone analyses with respect to loss or enhancement of color. Admittedly a larger and more diverse suite of gemstones should be investigated to confirm the results of the preliminary study. Aspects such as the safe X-ray dosage range and distance between source and sample should be calibrated. In addition, the use of a more sensitive method to detect subtle discoloration is advised, in order to make precise observations of the color changes after X-ray exposure. The averaging of spectral signatures obtained by several iterations would improve the quality of the data. The absorption of the blue region of the spectrum during irradiation for all gemstones, should also be studied.

The precision of the method has been demonstrated to be excellent. The resolution of the 3D images is a function of voxel size selection. Very large files are however created at low voxel size and can be cumbersome to work with. It is recommended that the selected resolution should be dictated by the minimum requirements of the particular study.

Subjectivity of the operator, particularly in the selection of fractures and segmentation as it influences the threshold values, could induce a bias in the volume calculation of filler material as it is done by visual inspection of the material. Several iterations may be required to obtain precise results however, operator experience with the method plays an equally important role. Subjectivity may prompt the development of an algorithm to standardize the selection process in the future.

X-ray micro computed tomography is a time-efficient, physically non-destructive, relatively low cost procedure to characterize external and internal features of gemstones and provide a 3D unique fingerprint. It is able to provide the gemstone industry, from mine to market, with a new method which complements existing procedures that can be routinely applied in the precise, non-biased characterization of gemstones. The benefits include the generation of a digital twin for record, insurance and forensic purposes.

Author Contributions: Conceptualization, A.R., R.H. and A.D.P.; Methodology, A.R., R.H. and A.D.P.; Software, A.D.P. and C.M.; Validation, A.R., A.D.P., R.H. and C.M.; Formal analysis, A.D.P. and C.M.; Investigation, C.M., R.H. and A.D.P.; Resources, A.D.P. and R.H.; Data curation, C.M. and A.D.P. All authors have read and agreed to the published version of the manuscript.

Funding: This research received no external funding.

Data Availability Statement: The data presented in this study are available on request from the corresponding author. The data are not publicly available due to large size of 20Gb per CT scan.

Acknowledgments: The CT scans were done at Stellenbosch University's CT Scanner Facility, an open access laboratory providing non-destructive X-ray computed tomography and a high performance image analysis services as part of the Central Analytical Facilities of the university [37]. Special thanks to the European Gemmological Laboratory South Africa for the lending a ruby on which analysis could be conducted. All participants in this project are gratefully acknowledged for their support in this effort. The constructive comments by the two reviewers greatly enhanced the quality of the manuscript. This is much appreciated.

Conflicts of Interest: The authors declare no conflict of interest.

References

1. Kammerling, R.C.; Koivula, J.I.; Kane, R.E. Gemstone enhancement and its detection in the 1980s. *Gems Gemol.* **1980**. [CrossRef]
2. McClure, S.F.; Smith, C.P. Gemstone enhancement and detection in the 1990s. *Gems Gemol.* **2000**. [CrossRef]
3. Breeding, C.; Shen, A.; Eaton-Magaña, S.; Rossman, G.; Shigley, J.; Gilbertson, A. Developments in gemstone analysis techniques and instrumentation during the 2000s. *Gems Gemol.* **2010**. [CrossRef]
4. Barone, G.; Bersani, D.; Lottici, P.P.; Mazzoleni, P.; Raneri, S.; Longobardo, U. Red gemstone characterization by micro-Raman spectroscopy: The case of rubies and their imitations. *J. Raman Spectrosc.* **2016**. [CrossRef]
5. Kiefert, L.; Hänni, H.A.; Chalain, J.-P.; Weber, W. Identification of filler substances in emeralds by infrared and Raman spectroscopy. *J. Gemmol.* **2000**. [CrossRef]
6. Shigley, J.E. Treated and synthetic gem materials. *Curr. Sci.* **2000**, *79*, 1566–1571.
7. McClure, S.F.; Smith, C.P.; Wang, W.; Hall, M. Identification and durability of lead glass-filled rubies. *Gems Gemol.* **2006**. [CrossRef]
8. Pardieu, V.; Lomthong, P.; Sturman, N. Lead Glass-Filled Star Rubies Reportedly from Madagascar. Available online: <https://www.gia.edu/UK-EN/ongoing-research/lead-glass-filled-star-rubies-reportedly-from-madagascar> (accessed on 31 October 2020).
9. Lowry, S. Using FTIR spectroscopy to analyze gemstones. *Am. Lab.* **2008**, *40*, 28–31.
10. Chen, V. Coloured Gemstones Rise in Demand among Jewellers and Investors as the Supply Dwindles. Available online: <https://www.scmp.com/magazines/style/article/1873766/coloured-gemstones-rise-demand-among-jewellers-and-investors-supply> (accessed on 31 October 2020).
11. CIBJO—The World Jewellery Confederation. Available online: <http://www.cibjo.org/code-of-ethics/> (accessed on 19 December 2020).
12. Ho, S.K. Analysis of impurity effects on the coloration of corundum by laser-induced breakdown spectroscopy (LIBS). *Appl. Spectrosc.* **2015**. [CrossRef]
13. Scarratt, K. A Discussion on Ruby-Glass Composites & Their Potential Impact on the Nomenclature in Use for Fracture-Filled or Clarity Enhanced Stones in General. Available online: <https://www.gia.edu/UK-EN/gia-news-research-nr41009> (accessed on 2 November 2020).
14. Clark, D. A Consumer's Guide to Gem Grading. Available online: <https://www.gemsociety.org/article/a-consumers-guide-to-gem-grading/> (accessed on 31 October 2020).

15. Branstrator, B. Analysis: The State of the Colored Stone Market. Available online: <https://www.nationaljeweler.com/diamonds-gems/supply/4803-the-state-of-the-colored-stone-market> (accessed on 31 October 2020).
16. Soldati, A.L.; Jacob, D.E.; Wehrmeister, U.; Hofmeister, W. Structural characterization and chemical composition of aragonite and vaterite in freshwater cultured pearls. *Mineral. Mag.* **2008**. [CrossRef]
17. Wehrmeister, U.; Goetz, H.; Jacob, D.E.; Soldati, A.; Xu, W.; Duschner, H.; Hofmeister, W. Visualization of the internal structures of cultured pearls by computerized X-ray microtomography. *J. Gemmol.* **2008**. [CrossRef]
18. Kawano, J. Observation of the internal structures of pearls by X-ray CT technique. *Gemmology* **2009**, *40*, 2–4.
19. Krzemnicki, M.; Friess, S.; Chalus, P.; Hänni, H.; Karamelas, S. X-ray computed microtomography: Distinguishing natural pearls from beaded and non-beaded cultured pearls. *Gems Gemol.* **2010**. [CrossRef]
20. Hänni, H.A. How much glass is in the ruby? *Ssef Facet.* **2009**, *16*, 8–9.
21. Bouts, A. Detection of Ruby Crystals in Marble Host Rock by X-ray Computed Tomography. *J. Gemmol.* **2014**. [CrossRef]
22. Sahoo, R.K.; Singh, S.K.; Mishra, B.K. Surface and bulk 3D analysis of natural and processed ruby using electron probe micro analyzer and X-ray micro CT scan. *J. Electron Spectrosc. Relat. Phenom.* **2016**. [CrossRef]
23. Cnudde, V.; Boone, M.N. High-resolution X-ray computed tomography in geosciences: A review of the current technology and applications. *Earth-Sci. Rev.* **2013**, *123*, 1–17. [CrossRef]
24. Rozendaal, A.; le Roux, S.G.; du Plessis, A.; Philander, C. Grade and product quality control by microCT scanning of the world class Namakwa Sands Ti-Zr placer deposit West Coast, South Africa: An orientation study. *Miner. Eng.* **2018**, *116*, 152–162. [CrossRef]
25. Rozendaal, A.; le Roux, S.G.; du Plessis, A. Application of microCT scanning in the recovery of endo-skarn associated scheelite from the Riviera Deposit, South Africa. *Miner. Eng.* **2018**, *116*, 163–178. [CrossRef]
26. Maire, E.; Withers, P.J. Quantitative X-ray tomography. *Int. Mater. Rev.* **2014**, *59*, 1–43. [CrossRef]
27. Du Plessis, A.; Boshoff, W.P. A review of X-ray computed tomography of concrete and asphalt construction materials. *Constr. Build. Mater.* **2019**, *199*, 637–651. [CrossRef]
28. Du Plessis, A.; Broeckhoven, C.; Guelpa, A.; Le Roux, S.G. Laboratory x-ray micro-computed tomography: A user guideline for biological samples. *GigaScience* **2017**, *6*, 1–11. [CrossRef] [PubMed]
29. Broeckhoven, C.; du Plessis, A. X-ray microtomography in herpetological research: A review. *Amphib. Reptil.* **2018**. [CrossRef]
30. Du Plessis, A.; Broeckhoven, C. Looking deep into nature: A review of micro-computed tomography in biomimicry. *Acta Biomaterialia* **2019**, *85*, 27–40. [CrossRef]
31. Du Plessis, A.; Yadroitsev, I.; Yadroitsava, I.; le Roux, S.G. X-ray Microcomputed Tomography in Additive Manufacturing: A Review of the Current Technology and Applications. *3D Print. Addit. Manuf.* **2018**. [CrossRef]
32. Roux, J. Classification of Diamonds by Microfocus X-Ray Computed Tomography. Unpublished Thesis, BSc honors, Department of Earth Sciences, Stellenbosch University, Stellenbosch, South Africa, 2012.
33. Du Plessis, A.; le Roux, S.G.; Rozendaal, A.; Tolken, A. X-ray tomography of cut and polished diamonds. *Gems Gemol.* Under review.
34. Du Plessis, A.; le Roux, S.G.; Rozendaal, A.; Tolken, A. X-ray tomography of cut and polished diamonds and gemstones. In Proceedings of the 35th International Geological Congress, Cape Town, South Africa, 27 August–4 September 2016.
35. Du Plessis, A.; le Roux, S.G.; Guelpa, A. The CT Scanner Facility at roux University: An open access X-ray computed tomography laboratory. *Nucl. Instrum. Methods Phys. Res. Sect. B Beam Interact. Mater. At.* **2016**, *384*, 42–49. [CrossRef]
36. Boas, F.E.; Fleischmann, D. CT artifacts: Causes and reduction techniques. *Imaging Med.* **2012**, *4*, 229–240. [CrossRef]
37. Le Roux, S.G.; du Plessis, A.; Rozendaal, A. The quantitative analysis of tungsten ore using X-ray microCT: Case study. *Comput. Geosci.* **2015**. [CrossRef]
38. Nassau, K. *Gemstone Enhancement*, 2nd ed.; Butterworth-Heinemann: Oxford, UK, 1984.
39. Pough, F.H.; Rogers, T.H. Experiments in X-ray irradiation of gem stones. *Am. Mineral. J. Earth Planet. Mater.* **1947**, *32*, 31–43.
40. The Laboratory Manual Harmonisation Committee LMHC Information Sheet # 3-Corundum. Available online: https://static1.squarespace.com/static/5bfb7e6cc8fed3bb9293bf3/t/5bfe9219f950b7627afb4cb0/1543410205254/LMHC+Information+Sheet_3_V9_2012.pdf (accessed on 21 December 2020).
41. Guelpa, A.; du Plessis, A.; Kidd, M.; Manley, M. Non-destructive Estimation of Maize (*Zea mays* L.) Kernel Hardness by Means of an X-ray Micro-computed Tomography (μ CT) Density Calibration. *Food Bioprocess Technol.* **2015**, *8*, 1419–1429. [CrossRef]
42. McClure, S.F.; Moses, T.M.; Tannous, M.; Koivula, J.I. Classifying emerald clarity enhancement at the GIA Gem Trade Laboratory. *Gems Gemol.* **1999**, *35*, 176–185. [CrossRef]
43. du Plessis, A.; Olawuyi, B.J.; Boshoff, W.P.; le Roux, S.G. Simple and fast porosity analysis of concrete using X-ray computed tomography. *Mater. Struct./Mater. Et Constr.* **2016**, *49*, 553–562. [CrossRef]
44. OGI Systems Ltd. Scanox CAD. Available online: <http://www.ogisystems.com/scanoxcad.html> (accessed on 21 December 2020).
45. OGI Systems Ltd. Clearex Gem. Available online: <http://www.ogisystems.com/clearexgem.html> (accessed on 21 December 2020).
46. Gemological Institute of America Colored Gemstone and Pearl Reports. Available online: <https://4cs.gia.edu/en-us/colored-gemstone-pearl-reports/> (accessed on 31 October 2020).
47. De Chiffre, L.; Carmignato, S.; Kruth, J.P.; Schmitt, R.; Weckenmann, A. Industrial applications of computed tomography. *Cirp Ann. Manuf. Technol.* **2014**, *63*, 655–677. [CrossRef]
48. Nassau, K. The Physics and Chemistry of Color: The Fifteen Causes of Color. *Color Res. Appl.* **1984**, *12*, 4–26. [CrossRef]